RSC Advances

PAPER

Cite this: *RSC Adv.*, 2020, **10**, 22120

Cellulose nanofiber-based electrode as a component of an enzyme-catalyzed biofuel cell†

Masato Tominaga, *[a] Kazufumi Kuwahara,[a] Masayuki Tsushida[b] and Kenji Shida[b]

Received 18th April 2020
Accepted 3rd June 2020

DOI: 10.1039/d0ra03476b

rsc.li/rsc-advances

Many types of flexible, wearable, and disposable electronic devices have been developed as chemical and physical sensors, and many solar cells contain plastics. However, because of environmental pollution caused by microplastics, plastic use is being reduced worldwide. We have developed an enzyme-catalyzed biofuel cell utilizing cellulose nanofiber (CNF) as an electrode component. The electrode was made conductive by mixing multi-walled carbon nanotubes with the CNF. This prepared biofuel cell was wearable, flexible, hygroscopic, biodegradable, eco-friendly, and readily disposable like paper. The CNF-based enzyme-catalyzed biofuel cell contained a flavin adenine dinucleotide-dependent glucose dehydrogenase bioanode and laccase biocathode. The maximum voltage and maximum current density of the biofuel cell were 434 mV and 176 μA cm^{-2}, respectively, at room temperature (15–18 °C). The maximum power output was 27 μW cm^{-2}, which was converted to 483 (±13) μW cm^{-3}.

1. Introduction

Many types of flexible, wearable, and disposable electronic devices have been developed for use as chemical and physical sensors, and many solar cells contain plastics that are difficult to biodegrade.[1–3] Realistically, it is very difficult to reuse the plastic from small devices. The world is currently moving towards reducing the use of plastics because of issues with microplastic pollution.[4,5] Therefore, it is preferable that wearable and disposable devices are made of environmentally friendly materials such as cellulose where possible. Cellulose is the most abundant carbohydrate on earth. Nanocellulose is made from wood, cotton, cellulose-rich materials, and organisms by mechanical methods or chemical dissolution.[6–11] Nanocellulose can be roughly classified as cellulose nanofiber (CNF), cellulose nanocrystals, and bacterial nanocellulose. Nanocellulose sheets are a flexible substrate for preparation of electronic devices and have good thermal and chemical stability.[6,10,11] They are also biodegradable, eco-friendly, and readily disposable like paper.[6,7] These properties are important for substrate materials used in wearable disposable devices.

Enzyme-catalyzed biofuel cells are considered an attractive power source for implants and microscale medical devices because of their biocompatibility and ability to operate under mild temperatures and near-neutral pH conditions.[12,13] These biofuel cells convert chemical energy into electrical energy under mild conditions using a redox enzyme as a catalyst to combine the oxidation reactions of organic fuels such as sugars and alcohols with the reduction reaction of oxygen. Furthermore, biofuel cells can operate as membrane-less fuel cells because of the high selectivity of the enzyme. Already, enzyme-catalyzed biofuel cells have been successfully implanted in rats, lobsters, snails, and insects.[14–17] These biofuel cells have enormous potential for application as energy harvesting power sources for use in wearable and disposable sensors. Many types of enzyme-catalyzed biofuel cells have been reported, including epidermal and contact lens fuel cells.[18–20] To realize practical use of enzyme-catalyzed biofuel cells as glucose fuel, flavin adenine dinucleotide-dependent glucose dehydrogenase (FAD-GDH) has been used as an oxidation catalyst for glucose. FAD-GDH is oxygen insensitive,[21–26] which is advantageous for its use as an anode in biological fuel cells. Furthermore, hydrogen peroxide, which can be generated from oxygen reduction in oxygen sensitive enzymes, is not produced. Hydrogen peroxide can be toxic in single-compartment fuel cells. A disadvantage of FAD-GDH is that it requires an electron transfer mediator between the enzyme and an electrode because direct electron transfer is impossible.[21–26] This requirement induces kinetic and thermodynamic losses compared with direct electron transfer.

In this study, we report the performance of a CNF-based electrode as a component of an enzyme-catalyzed biofuel cell. The anodic system uses FAD-GDH and 9,10-phenanthrenequinone as a mediator, and the cathodic system uses laccase. Multi-walled carbon nanotubes (MWCNTs) were included to give conductivity to the CNF. CNF reportedly

[a]*Department of Chemistry and Applied Chemistry, Saga University, Saga 840-8502, Japan. E-mail: masato@cc.saga-u.ac.jp*

[b]*Faculty of Engineering, Kumamoto University, Kumamoto 860-8555, Japan*

† Electronic supplementary information (ESI) available. See DOI: 10.1039/d0ra03476b

promotes proton conductivity.[10,27] This property could have a buffering effect for large and rapid changes in the pH near the anode and cathode of the biofuel cell during an enzymatic reaction. To the best of our knowledge, investigations of enzyme-catalyzed biofuel cells prepared using CNF have been limited,[28] although there have some reports of traditional paper electrodes containing CNF.[29,30] CNF may not be the best material for use in the electrode, but in consideration of balancing environmental, eco-friendliness, and performance demands, it is necessary to consider the use of the CNF-based electrodes in wearable enzyme fuel cells.

2. Experimental

2.1 Materials

Nanoforest-S BB made from bamboo using the aqueous counter collision (ACC) method was used as the CNF, and was kindly supplied by Chuetsu Pulp and Paper Co., Ltd. (Tokyo, Japan). The ACC-treated CNF has both surface properties of hydrophobic and hydrophilic.[31,32] MWCNTs (outer diameter 10 (±1) nm, inner diameter 4.5 (±0.5) nm, and length 3–6 μm) was obtained from Sigma-Aldrich. Fungal laccase (Lac) from *Trametes* sp. (Enzyme Commission number EC 1.10.3.2) was obtained from Amano Enzyme (Nagoya, Japan) and purified according to an established method.[33] The purity of Lac was confirmed by SDS-PAGE, which gave a single band at approximately 63 kDa.[30] The Lac concentration was determined from its molar absorption coefficient of 5700 (mol dm^{-3})$^{-1}$ cm^{-1} at 614 nm.[34] FAD-GDH (EC 1.1.5.9) was kindly gifted by Ikeda Food Research Co., Ltd. (Hiroshima, Japan). Sodium cholate (SC) was obtained from FUJIFILM Wako Pure Chemical Industries (Osaka, Japan). 9,10-Phenanthrenequinone for use as a mediator for FAD-GDH was obtained from FUJIFILM Wako Pure Chemical Industries. Potassium hexacyanoferrate(III) ($K_3[Fe(CN)_6]$) was obtained from FUJIFILM Wako Pure Chemical Industries. Water was purified with a Millipore Milli-Q water system. All other chemical reagents were of analytical grade and were used without further purification.

2.2 Preparation of CNF sheet and electrically conductive MWCNT/CNF sheet

The CNF sheet was prepared as follows. First, 300 mg of the CNF was dispersed in 20 mL of water using an ultrasonic homogenizer (Sonifier 450AA, Branson Ultrasonics Division of Emerson Japan Ltd). Next, 10 mL of this CNF dispersion was spread on a Teflon sheet (4 cm × 10 cm) and air dried. The dry CNF sheet was cut into 15 × 15 mm squares. An electrically conductive MWCNT/CNF sheet was prepared as follows. First, 8 mg of CNF and 2 mg of MWCNTs were dispersed in 10 mL of water using an ultrasonic homogenizer. Next, 2.5 mL of the MWCNT/CNF dispersion was cast to a size of 10 × 5 mm on the previously prepared CNF sheet under heating at approximately 200 °C on a hotplate. An electrode for the enzyme-catalyzed biofuel cell was prepared by attaching two electrically conductive MWCNT/CNF sheets so that the MWCNT surfaces were not facing each other (Scheme 1). The thickness of the electrode for the enzyme-catalyzed biofuel cell was 60 (±10) μm.

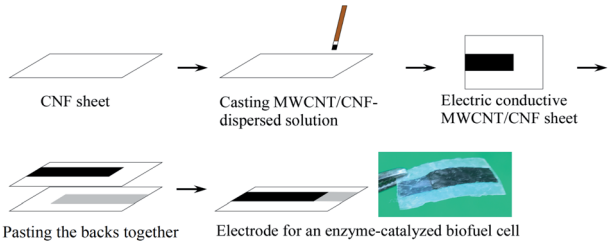

Scheme 1 Schematic illustration of electrode preparation for the enzyme-catalyzed biofuel cell.

2.3 Enzyme-catalyzed biofuel cell

The cathode of the enzyme-catalyzed biofuel cell was prepared by drop-coating functionalization as follows (Scheme S1 in ESI†). Both surfaces of the electrode for the enzyme-catalyzed biofuel cell were treated with UV-ozone for 3 min to remove organic contaminants.[35] Next, 10 μL of 0.2% (w/v) SC was cast on the electrically conductive part of the sheet (10 × 5 mm) on one surface of the electrode (SC/MWCNT/CNF sheet) and dried under vacuum (0.04 MPa). Then, 10 μL of acetate buffer solution (pH 5) containing 10 μmol dm^{-3} Lac was cast over this and also dried under vacuum. For preparation of the biofuel cell anode, the other surface of the electrode was modified with 9,10-phenanthrenequinone and FAD-GDH. First, 10 μL of an ethanol solution of 1.6 mmol dm^{-3} 9,10-phenanthrenequinone was cast on the electric conductive part (10 × 5 mm) and dried under vacuum (0.04 MPa). Then, 10 μL of 0.1 mol dm^{-3} acetate buffer solution (pH 5) containing 39 μmol dm^{-3} FAD-GDH was cast over this and also dried under vacuum.

2.4 Instrumentation

Scanning electron microscopy (SEM) imaging was performed using a JSM-7600F (JEOL, Japan). Each sample was coated with approximately 5 nm of osmium by sputtering before the SEM measurements. Field-emission transmission electron microscopy (FE-TEM) was performed using a Tecnai F-20 (Philips Electron Optics, Netherlands). UV-ozone treatment was performed using a UV–ozone system (OC-2503, Eye Graphics Co., Japan).

Fourier transform infrared spectroscopy (FT-IR) was performed using a Vertex 70-S (Bruker, Japan). A small portion of the mixed dispersion of MWCNTs and CNF was mixed with 200 mg of dry KBr powder to prepare transparent discs for analysis by FT-IR. KBr discs of the CNF sample were also prepared. Voltammetry measurements were performed with an electrochemical analyzer (ALS/CHI model 600A) with a conventional three-electrode cell. The reference electrode was Ag/AgCl/saturated KCl (+199 mV *vs.* the normal hydrogen electrode) and a platinum plate was used as the counter electrode. All potentials are reported with respect to Ag/AgCl/saturated KCl at 25 °C. Cyclic voltammograms were simulated with cyclic voltammetry simulation software (DigiSim 2.0, Bioanalytical Systems, Tokyo, Japan).[36]

3. Results and discussion

3.1 TEM, SEM, and FT-IR results

The mixed dispersion of MWCNTs and CNF did not show any separation or sedimentation after more than 2 weeks. Fig. 1

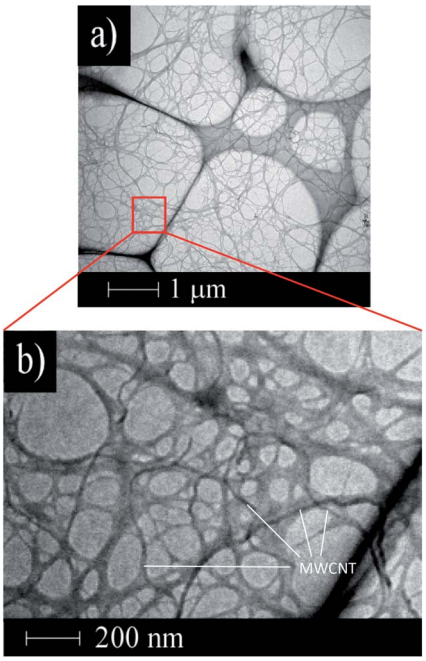

Fig. 1 TEM images of the dispersed MWCNT/CNF sample. Wide range (low magnification) (a) and narrow range (high magnification) images (b).

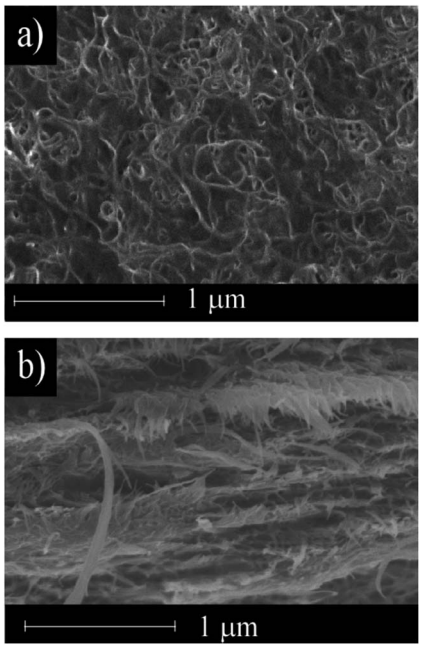

Fig. 3 SEM images of the surface (a) and cross section (b) of the MWCNT/CNF sheet.

shows TEM images of the dispersed sample on a TEM grid. In these images, the CNF is dispersed in clusters measuring 10–50 nm in diameter, which is in good agreement with a previous report.[32] Interestingly, the dispersed MWCNTs are included into the CNF clusters, which show the CNF assists with dispersion of the MWCNTs. The FT-IR spectra of the MWCNT/CNF and CNF are shown in Fig. 2. A characteristic band assigned to –OH stretching of intramolecular hydrogen bonds in CNF located was observed at 3400 cm^{-1}. A peak located at around 2900 cm^{-1} was assigned to the C–H stretching.[8,9] This peak was very small in the MWCNT/CNF sample. A band located at around 1600 cm^{-1} was assigned to –OH groups of water absorbed by CNF. CNF characteristic bands appeared around 1430 cm^{-1} and 1373 cm^{-1} and were assigned to $-CH_2$ symmetric bending and C–H bending changing, respectively. A band at around 1050 cm^{-1} was assigned to C–O stretching, and one at 896 cm^{-1} was assigned to C–H bending and $-CH_2$ stretching. Interestingly, for the MWCNT/CNF sample, the intensities of the bands assigned to vibrations of C–H (2900 cm^{-1}), $-CH_2$ (1430 and 896 cm^{-1}), and C–H (1373 and 896 cm^{-1}) were much smaller or absent. These results were in good agreement with the TEM results and showed that the MWCNT surface was covered with hydrophobic CNF. Formation of this supramolecular structure leads to good and stable dispersion of the MWCNTs in the aqueous solution.

Fig. 3 shows the morphology of the surface and a cross section of the electrically conductive MWCNT/CNF sheet. The surface morphology was similar to carpet fiber. Random fibers with diameters of a few dozen nanometers were observed. The cross-section image (Fig. 3b) showed the structure was formed of many layers with nanometer-scale thickness. This laminated structure could have high conductivity in the horizontal dimension.

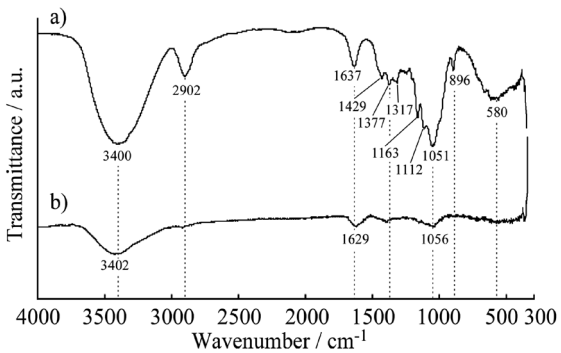

Fig. 2 FT-IR spectra of CNF (a) and MWCNT/CNF (b).

3.2 Electrochemical characterization

To evaluate the electrical conductivity of the MWCNT/CNF sheet, cyclic voltammetry of $[Fe(CN)_6]^{3-}$ in 1 mol dm^{-3} KCl solution (pH 7) was conducted (Fig. 4a). Separation between the anodic and cathodic peaks was approximately 500 mV, resulting in a slow redox reaction. The used MWCNT had many structural defects, which resulted in the presence of oxygen-containing hydrophilic functional groups, such as –C=O, –COOH, and –C–OH, on the MWCNT surface. These negatively charged functional groups in a neutral solution would inhibit the redox reaction of $[Fe(CN)_6]^{3-}$. Adsorption of $[Fe(CN)_6]^{3-}$ on the surface of the MWCNT/CNF sheet was not observed. In fact, the redox reaction was a perfect diffusion-controlled process because the

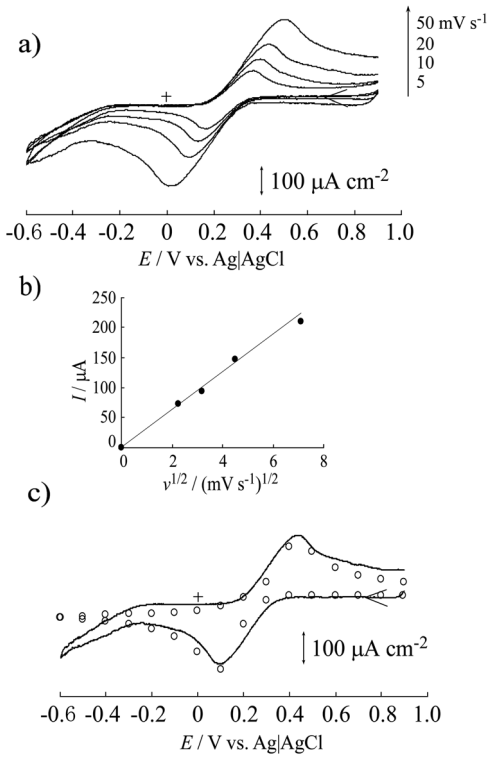

Fig. 4 Cyclic voltammograms of 1 mmol dm^{-3} $[Fe(CN)_6]^{3-}$ at the MWCNT/CNF sheet in 1 mol dm^{-3} KCl solution (pH 7) at various potential sweep rates (a), and plot of the cathodic peak current *versus* the square root of the potential sweep rate (b). Panel (c) shows the background subtracted voltammogram (solid line) at a potential sweep rate of 20 mV s^{-1} and the simulated voltammogram (open circle) using the following parameters: active surface area, 0.4 cm^2; redox potential, $E^{\circ\prime} = 0.27$; diffusion coefficient, $D = 1.4 \times 10^{-5}$ cm^2 s^{-1}; heterogeneous electron transfer rate, $k^{\circ\prime} = 1.5 \times 10^{-5}$ cm s^{-1}; and transfer coefficient, $\alpha = 0.5$.

peak current was proportional to the square root of the potential sweep rate (Fig. 4b). To analyze the redox reaction, a voltammetric simulation was performed.[35] This gave a simulated voltammogram that was a good fit for the background (electrical double layer capacitance) subtracted voltammogram (Fig. 4c). The redox potential ($E^{\circ\prime}$) and diffusion coefficient (D) were 0.27 (*vs.* Ag/AgCl/saturated KCl) and 1.4×10^{-5} cm^2 s^{-1}, respectively, and were in good agreement with previously reported values.[34] The heterogeneous electron transfer rate ($k^{\circ\prime}$) was estimated to be 1.5×10^{-5} cm s^{-1}, which was almost 1/100th that of the previously reported value.[35] Surprisingly, the estimated electrode surface area was 0.4 cm^2 even though the apparent electrode surface area was only 0.3 cm^2. The larger effective surface area could be attributed to the carpet fiber-like morphology of the surface. This result would be caused by limitation of the electrochemically active surface area of the MWCNTs because of CNF covering the MWCNT surface.

3.3 Lac-modified and FAD-GDH-modified MWCNT/CNF sheets

Fig. 5a shows the cyclic voltammograms of the Lac immobilized SC/MWCNT/CNF sheet in 0.1 mol dm^{-3} acetate buffer solution

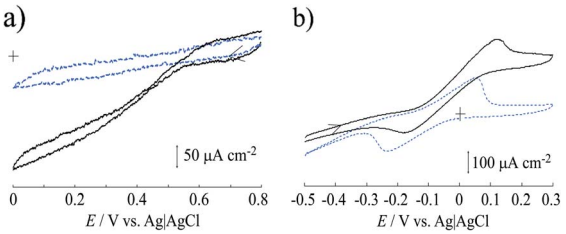

Fig. 5 (a) Lac direct bioelectrocatalytic current obtained at the SC-modified MWCNT/CNF sheet in 0.1 mol dm^{-3} acetate buffer solution (pH 5) containing O_2 (solid line) and Ar gas (broken line) at a potential sweep rate of 10 mV s^{-1}. (b) Mediated catalytic current of FAD-GDH in the 9,10-phenanthrenequinone-modified MWCNT/CNF sheet in 0.1 mol dm^{-3} acetate buffer solution (pH 5) in the presence (solid line) and absence (broken line) of 30 mmol dm^{-3} glucose at a potential sweep rate of 10 mV s^{-1}. Temperature range: 15–18 °C.

(pH 5). After injecting O_2 gas, the cathodic catalytic current from the direct electron transfer reaction of Lac had a high positive potential of around 0.6 V (*vs.* Ag/AgCl/saturated KCl), which was in good agreement with our previous results for a single-walled carbon nanotube-modified electrode.[33,37] This result means that the Lac immobilized SC/MWCNT/CNF sheet has potential for use as a cathode in an enzymatic biofuel cell.

For development of an anode for the biofuel cell, cyclic voltammetry of the MWCNT/CNF sheet modified with FAD-GDH and 9,10-phenanthrenequinone was performed (Fig. 5b). In the absence of glucose, 9,10-phenanthrenequinone gave one coupled redox reaction with an anodic and cathodic peaks at approximately 0.05 and −0.25 V. The redox potential ($E^{\circ\prime}$) was estimated to be −0.10 V from the potential midway between the anodic and cathodic peak potentials. Taking into account the pH difference, the obtained $E^{\circ\prime}$ was similar to that previously reported for a 9,10-phenanthrenequinone-modified glassy carbon electrode prepared by a simple drop-casting method.[38] The peak current value as a function of the potential sweep rate indicated that the redox reaction of 9,10-phenanthrenequinone was a diffusion-controlled process (Fig. S1 in ESI†). A previous reported stated that 9,10-phenanthrenequinone reacted with adsorbed species occurred *via* π–π stacking force between 9,10-phenanthrenequinone and the graphitic carbon electrode.[38,39] The difference between our result and the previous report could be caused by the dispersion of MWCNT with the CNF. As described in the above section, the MWCNT surface is covered with CNF because of hydrophobic interactions between the two components. This means that the hydrophilic part of CNF is facing the solution and may inhibit the adsorption of 9,10-phenanthrenequinone. After injection of glucose, we found that the catalytic current increased from approximately −0.15 V, which indicated that 9,10-phenanthrenequinone could act as a mediator for the FAD-GDH used in this study. This result means that the FAD-GDH-modified MWCNT/CNF sheet has potential for use as an anode against the Lac-modified MWCNT/CNF sheet.

Fig. 6 shows a diagram integrating the positive potential sweeping voltammogram for the FAD-GDH reaction and the negative potential sweeping voltammogram for the Lac

reaction. This diagram illustrates two important findings. First, the ideal maximum obtained voltage (potential difference) is approximately 700 mV when FAD-GDH and the Lac-modified MWCNT/CNF sheet are used as the anode and cathode of the enzyme-catalyzed biofuel cell. Second, a theoretical maximum current of approximately 170 μA cm^{-2} can be expected for the biofuel cell.

3.4 Enzyme-catalyzed biofuel cell

An enzyme-catalyzed biofuel cell utilizing FAD-GDH and Lac was developed that had a single compartment with a mixed catholyte and anolyte at pH 5 (0.1 mol dm^{-3} acetate buffer solution) in 30 mmol dm^{-3} glucose. Fig. 7a shows a photograph of the manufactured actual enzyme-catalyzed biofuel cell. This biofuel cell was very flexible, very thin (thickness of *ca.* 60 μm), and could adsorb glucose from solution. Therefore, the MWCNT/CNF sheet is useful as a platform electrode for wearable enzyme-catalyzed biofuel cells and could be attached to the skin. The whole reaction of the biofuel cell is shown in Fig. 7b. An oxidation reaction of two electrons per glucose molecule occurs on the anode side, and a four-electron reduction of water from oxygen occurs on the reduction side. Fig. 7c shows the polarization and power curves of the biofuel cell prepared with the FAD-GDH bioanode and Lac biocathode. The biofuel cell had maximum values for the voltage, current density, and power output of 434 mV, 176 μA cm^{-2}, and 27 μW cm^{-2} under an atmosphere at room temperature (15–18 °C). The obtained current value was same to the expected value (170 μA cm^{-2}). However, the obtained voltage value was about 60% of the value predicted from the separate results for the anode and the cathode (*ca.* 700 mV). The most probable cause for this decrease is a local change in the pH near the electrode interface because of the enzymatic reaction.[40] When the anode and the cathode

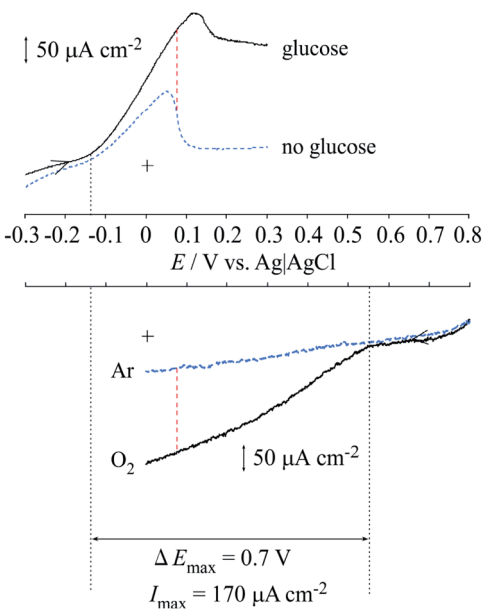

Fig. 6 Diagram integrating the voltammograms of the anodic current from FAD-GDH and cathodic current from Lac.

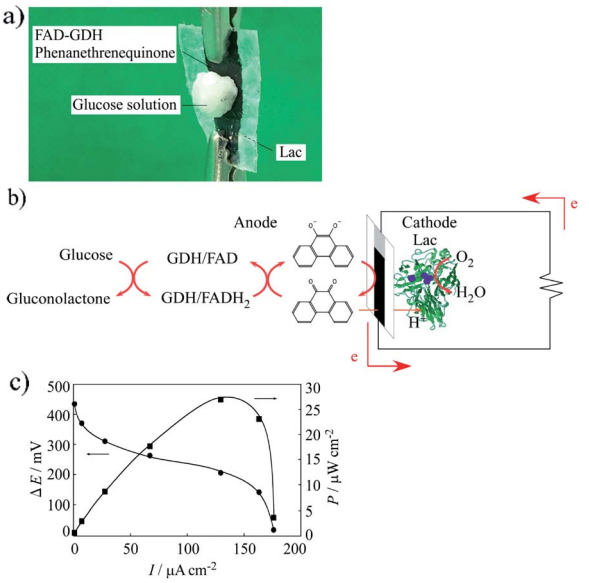

Fig. 7 (a) Photograph of the manufactured actual enzyme-catalyzed biofuel cell with a FAD-GDH bioanode and Lac biocathode. (b) Schematic illustration of the whole reaction of the enzyme-catalyzed biofuel cell. (c) The obtained polarization and power curves of the biofuel cell with 30 mmol dm^{-3} glucose in 0.1 mol dm^{-3} acetate buffer solution (pH 5) at room temperature (15–18 °C).

were measured separately, the measurement was performed in a cell containing about 20 mL of the buffer solution. Therefore, the pH change at the electrode interface because of the enzyme reaction could be suppressed to some extent. By contrast, in the case of the enzyme-catalyzed biofuel cell, it is expected that sufficient buffer capacity cannot be exhibited when a very small volume of buffer solution (several tens of microliters) permeates into the sheet.

Considering the thickness (60 (±10) μm) of the fuel cell of the MWCNT/CNF sheet, the power generation can be written as 483 (±13) μW cm^{-3}. The obtained maximum power output is *ca.* 880% higher than the previous result obtained from an enzyme-catalyzed biofuel cell containing a CNF/CNT electrode.[28] To the best of our knowledge, the investigation of the biofuel cell prepared using CNF have been very limited,[28] and the power generation is still limited compared with that obtained from an enzyme-catalyzed biofuel cells containing a buckypaper electrode, gold nanoparticle-modified electrode, and redox polymer hydrogel,[19–24] however the CNF having features such as biodegradable, flexible and eco-friendly have sufficient potential not only as the biofuel cells but also as a wide range of future electrode materials.

4 Conclusions

A nanocellulose-based electrode was manufactured using MWCNTs as an electrically conductive material. CNF prepared by the aqueous counter collision method gave good dispersion of the MWCNTs. This dispersion mechanism was observed in FT-IR results, which indicated that the graphitic surface of the MWCNTs was covered with CNF. The enzyme-catalyzed biofuel

cell was utilized as a FAD-GDH bioanode and Lac biocathode. Both the maximum voltage (434 mV) and maximum current density (176 μA cm^{-2}) under an atmosphere at room temperature (15–18 °C). The maximum power output was 27 μW cm^{-2}, which was converted to 483 (±13) μW cm^{-3}. The manufactured CNF-based sheet was soft and flexible, hygroscopic, biodegradable, eco-friendly, and disposable. These features are ideal for an electrode material that is used in wearable enzyme-catalyzed biofuel cells, even though the output power is still limited.

Conflicts of interest

There are no conflicts to declare.

Acknowledgements

We thank Chuetsu Pulp & Paper Co., Ltd. (Tokyo, Japan) for samples of Nanoforest-S BB and Ikeda Food Research Co., Ltd. (Hiroshima, Japan) for samples of FAD-GDH. We thank Gabrielle David, PhD, from Edanz Group (http://www.edanzediting.com/ac) for editing a draft of this manuscript.

References

1 S. Choi, H. Lee, R. Ghaffari, T. Hyeon and D.-H. Kim, *Adv. Mater.*, 2016, **28**, 4203–4218.
2 L. Wen, F. Li and H.-M. Cheng, *Adv. Mater.*, 2016, **28**, 4306–4337.
3 S. Khan, L. Lorenzelli, S. Ravinder and R. S. Dahiya, *IEEE Sens. J.*, 2015, **15**, 3164–3185.
4 A. Ganesh Kumar, K. Anjana, M. Hinduja, K. Sujitha and G. Dharani, *Mar. Pollut. Bull.*, 2020, **150**, 110733.
5 X. Chang, Y. Xue, J. Li, L. Zou and M. Tang, *J. Appl. Toxicol.*, 2020, **40**, 4–15.
6 T. C. Mokhena and M. J. John, *Cellulose*, 2020, **27**, 1149–1194.
7 I. Siró and D. Plackett, *Cellulose*, 2010, **17**, 459–494.
8 S. Sulaiman, M. N. Mokhtar, M. N. Naim, A. S. Baharuddin and A. Sulaiman, *Appl. Biochem. Biotechnol.*, 2015, **175**, 1817–1842.
9 J. Rostami, A. P. Mathew and U. Edlund, *Molecules*, 2019, **24**, 3147.
10 C. Vilela, A. J. D. Silvestre, F. M. L. Figueiredo and C. S. R. Freire, *J. Mater. Chem. A*, 2019, **7**, 20045–20074.
11 M. S. Islam, L. Hen, J. Sisler and K. C. Tam, *J. Mater. Chem. B*, 2018, **6**, 864–883.
12 S. C. Barton, J. Gallaway and P. Atanassov, *Chem. Rev.*, 2004, **104**, 4867–4886.
13 C. Laane, W. Pronk, M. Franssen and C. Veeger, *Enzyme Microb. Technol.*, 1984, **6**, 165–168.
14 A. Zebda, S. Cosnier, J.-P. Alcaraz, M. Holzinger, A. Le Goff, C. Gondran, F. Boucher, F. Giroud, K. Gorgy, H. Lamraoui and P. Cinquin, *Sci. Rep.*, 2013, **3**, 370–375.
15 K. MacVittie, J. Halámek, L. Halámková, M. Southcott, W. D. Jemison, R. Lobel and E. Katz, *Energy Environ. Sci.*, 2013, **6**, 81–86.
16 L. Halámková, J. Halámek, V. Bocharova, A. Szczupak, L. Alfonta and E. Katz, *J. Am. Chem. Soc.*, 2012, **134**, 5040–5043.
17 M. Rasmussen, R. E. Ritzmann, I. Lee, A. J. Pollack and D. Scherson, *J. Am. Chem. Soc.*, 2012, **134**, 1458–1460.
18 W. Jia, G. Valdés-Ramírez, A. J. Bandodkar, J. R. Windmiller and J. Wang, *Angew. Chem., Int. Ed.*, 2013, **52**, 7233–7236.
19 Y. Ogawa, K. Kato, T. Miyake, K. Nagamine, T. Ofuji, S. Yoshino and M. Nishizawa, *Adv. Healthcare Mater.*, 2015, **4**, 506–510.
20 D. Pankratov, E. González-Arribas, Z. Blum and S. Shleev, *Electroanalysis*, 2016, **28**, 1250–1266.
21 A. J. Gross, X. Chen, F. Giroud, C. Abreu, A. L. Goff, M. Holzinger and S. Cosnier, *ACS Catal.*, 2017, **7**, 4408–4416.
22 D. Fapyane, S.-J. Lee, S.-H. Kang, D.-H. Lim, K.-K. Cho, T.-H. Nam, J.-P. Ahn, J.-H. Ahn, S.-W. Kim and I. S. Chang, *Phys. Chem. Chem. Phys.*, 2013, **15**, 9508–9512.
23 F. Gholami, A. Navaee, A. Salimi, R. Ahmadi, A. Korani and R. Hallaj, *Sci. Rep.*, 2018, **8**, 1–14.
24 C. Hou, Q. Lang and A. Liu, *Electrochim. Acta*, 2016, **211**, 663–670.
25 R. D. Milton, D. P. Hickey, S. Abdellaoui, K. Lim, F. Wu, B. Tan and S. D. Minteer, *Chem. Sci.*, 2015, **6**, 4867–4875.
26 B. Reuillard, A. Le Goff, S. C. Agne, M. Holzinger, A. Zebda, C. Gondran, K. Elouarzaki and S. Cosnier, *Phys. Chem. Chem. Phys.*, 2013, **15**, 4892–4896.
27 T. D. O. Gadim, F. J. A. Loureiro, C. Vilela, N. Rosero-Navarro, A. J. D. Silvestre, C. S. R. Freire and F. M. L. Figueiredo, *Electrochim. Acta*, 2017, **233**, 52–61.
28 P. Lv, Q. Feng, Q. Wang, D. Li, J. Zhou and Q. Wei, *Fibers Polym.*, 2016, **17**, 1858–1865.
29 I. Shitanda, M. Momiyama, N. Watanabe, T. Tanaka, S. Tsujimura, Y. Hoshi and M. Itagaki, *ChemElectroChem*, 2017, **4**, 2460–2463.
30 S. Rengaraj, Á. Cruz-Izquierdo, J. L. Scott and M. D. Lorenzo, *Sens. Actuators, B*, 2018, **265**, 50–58.
31 T. Kondo, R. Kose, H. Naito and W. Kasai, *Carbohydr. Polym.*, 2014, **112**, 284–290.
32 S. Yokota, K. Kamada, A. Sugiyama and T. Kondo, *Carbohydr. Polym.*, 2019, **226**, 115293.
33 M. Tominaga, A. Sasaki, M. Tsushida and M. Togami, *New J. Chem.*, 2017, **41**, 231–236.
34 R. Santucci, T. Ferri, L. Morpurgo, I. Savini and L. Avigliano, *Biochem. J.*, 1998, **332**, 611.
35 M. Tominaga, N. Hirata and I. Taniguchi, *Electrochem. Commun.*, 2005, **7**, 1423–1428.
36 M. Rodolph, D. P. Reddy and S. W. Feldberg, *Anal. Chem.*, 1994, **66**, 589A–600A.
37 M. Tominaga, A. Sasaki and M. Togami, *Anal. Chem.*, 2015, **87**, 5417–5421.
38 K. S. Shalini and A. S. A. Kumar, *Analyst*, 2018, **143**, 3114–3123.
39 W. Wang, Y. Yang, X. Wang, Y. Zhou, X. Zhang, L. Qiang, Q. Wang and Z. Hu, *New J. Chem.*, 2019, **43**, 6380–6387.
40 M. Nemoto, K. Sugihara, T. Adachi, K. Murata, K. Shiraki and S. Tsujimura, *ChemElectroChem*, 2019, **6**, 1028–1031.